

NUMERICAL SIMULATION OF COHESIVE SEDIMENT TRANSPORT IN JAKARTA BAY

I. M. Radjawane¹ And F. Riandini²

Abstract. The 3D-numerical model has been applied to simulate the current circulation and cohesive sediment transport in the Jakarta Bay, Indonesia. Sediment load comes from 3 river mouths i.e. Angke River, Karang River, and Ancol River. The model was simulated to analyze the effect of tidal current and river discharge. A constant westerly and easterly wind was used as input of the model to see the influence of monsoonal season. The numerical results showed that the tidal current flows from east to western part of the bay during ebb tide and vice versa during flood tide. The surface current circulation was dominantly influenced by the tidal current compared with the wind and river discharge effects. High turbidity level was found near the river mouths with the range of 50 to 100 mg/l. This high sediment concentration was caused by the effect of sediment load from the river upstream. In the offshore area of the bay the sediment concentration decreases up to 10 mg/l. The movement of sediments followed the current circulations. During the flood tide, the sediment concentration from the mouth of Angke River moved to the western part of the bay. Model simulated for increasing the river discharge into two times showed that the sediment distributed to the offshore direction two times longer compare with the normal debit. The transport of sediment from the Angke and Karang Rivers to the offshore area reached > 6 km, while it just reached $\pm 2,5$ km from the Ancol River .

Keywords: *3D-numerical model, Cohesive sediment, Effect of tidal current and river discharge*

1. Introduction

Jakarta Bay is located at western side of northern part of Java Island, a shallow bay with an average depth of about 15 m, an area of 514 km², and a shoreline about 72 km long. The bay receives highly polluted water from 19 rivers that run through the Jakarta Metropolitan Area (JMA) and poured out into the Java Sea (UNESCO, 2000).

The current circulation in this bay is controlled mainly by the three physical processes, i.e. tides, wind and river discharges (Koropitan, et. al., 2009 and Rachmayani, 2004). Tides are dominated by the diurnal components, especially the K₁ component coming from Flores Sea and

through Java Sea and resulting the co-oscillation tides in the central part of Java Sea. The monsoon wind system prevails over the Java Sea that consists of the northwest monsoon during December to February, southeast monsoon during June to August, and two transitional monsoons. There are several rivers, such as the Citarum, Ciliwung, Angke, Ancol, and Karang Rivers. The physical processes affected the dynamics of sedimentation and erosion in this area. Bathymetry and coastline change is one issue in JMA. Wind direction and river discharges are seasonal based data.

¹ Oceanography Department, Faculty of Earth Sciences and Technology, Bandung Institute of Technology.
E-mail: ivonnemr@geoph.itb.ac.id

² Research Institute of Water Resources and Development, Bandung, Indonesia.

Further, this area becomes worse and causes the sea floor and coastline surrounding the Jakarta Bay changed due to the anthropogenic effect, i.e. human activities as reported from UNESCO (2000). Large scale sand extraction started with harbour dredging in the Jakarta Bay area. The dredged material was generally dumped elsewhere in the bay and continuation of sand extraction for building started on a small scale and was carried out manually in the 1970s and has intensified yearly in order to provide construction materials. Mangrove area has been transformed into reclamation area for luxury residences, commercial activities, and industrial zones. Based on comparison satellite image between 1971 and 2004, there are 80% of land use changes from vegetative area into urban area and almost at the coastal area (Koropitan, 2009).

A comprehensive study to understand the spatial and temporal distribution of cohesive sediments in this bay due to the main physical processes is needed. In this study, the monsoon effect, tides, and river discharges are simulated into a hydrodynamic model to get a more clear understanding concerning with current circulation in this bay. The dynamic of sedimentation and erosion processes is simulated with a sediment transport model. Several scenarios based on generating forces of the current circulation are conducted to understand the variation and dynamics of seasonal distribution.

2. Model Descriptions

A three-dimensional finite difference model system for hydrodynamic and cohesive sediment transport, ECOMSED (HydroQual, 2002), is used in this simulation. This model solves the Navier-Stokes equations with free surface boundary conditions and the advection-diffusion equations of the temperature, salinity, and any other variable. To

simulate the cohesive sediment transport, the ECOMSED model was improved by applying flocculation and consolidation processes, resulting in the following three specific module developments.

Suspended Sediment Module

The transport of suspended sediment is described by the following advection-diffusion equation:

$$\frac{\partial c}{\partial t} + \frac{\partial}{\partial x_i}((u_i - \delta_{is} w_s) c) = \frac{\partial}{\partial x_i} \left(A_H \frac{\partial c}{\partial x_i} \right) + \frac{\partial}{\partial x_2} \left(A_H \frac{\partial c}{\partial x_2} \right) + \frac{\partial}{\partial x_3} \left(K_H \frac{\partial c}{\partial x_3} \right) \quad (1)$$

where, c : concentration of the suspended sediment, u_i : velocity components. A_H : the horizontal diffusivity and K_H : the vertical eddy diffusivity.

At the water surface, z_s , the net sediment flux is zero. At the sediment-water interface, z_b , the flux is estimated by the rates of erosion and deposition, $F_{erosion}$ and $F_{deposition}$. The bottom boundary condition can therefore be formulated as follows:

$$\left\{ (u_i - w_s) c - K_H \frac{\partial c}{\partial x_3} \right\}_{x_3=z_s} = 0 \quad \text{and} \\ \left\{ (u_i - w_s) c - K_H \frac{\partial c}{\partial x_3} \right\}_{x_3=z_b} = E_{b,c} \quad (2)$$

with $E_{b,c} = F_{erosion} + F_{deposition}$.

The erosion rate is represented by Partheniades's formulation (Partheniades, 1965) as:

$$F_{erosion} = M \left(\frac{\tau_b}{\tau_e} - 1 \right) \quad (3)$$

where, M is a positive empirical erosion parameter, τ_b is the bed shear stress, τ_e is the critical shear stress for erosion, is a function of the concentration of the top bed layer, which itself is given by the state of consolidation. The erosion coefficient M may also be function of the concentration. The deposition rate is calculated according to Krone's formula (Krone, 1962):

$$F_{deposition} = P_d w_s c \quad (4)$$

where P_d is the probability for deposition described by,

$$P_d = 1 - \left(\frac{\tau_b}{\tau_d} \right) \quad (5)$$

where τ_d is the critical shear stress for deposition.

Flocculation Module

2.2.1. Relation between Settling Velocity and Floc Size

Winterwerp (1998) developed three-dimensional Eulerian model of the evolution of the settling velocity of fine-grained cohesive sediment in turbulent open channel flow:

$$w_{sr} = \frac{\alpha}{18\beta} \frac{(\rho_s - \rho_w)g}{\mu} D_p^{3-n_f} \frac{D^{n_f-1}}{1 + 0.15 Re_p^{0.687}} \quad (6)$$

which D is the actual floc size, D_p is the diameter of the primary particle, and n_f is fractal dimension for sediment particles. α and β are coefficients depending on the sphericity of the particles, and Re is the particle Reynolds number.

Mud flocs seldom settle as individual particles. When their concentration becomes high enough, the settling flocs start to hinder each other in their movement, generally known as hindered settling. The effective settling velocity w_s in suspension of cohesive sediment affected by the process of hindered settling defined as:

$$w_s = w_{sr} \frac{(1 - \phi_*) (1 - \phi_p)}{1 + 2.5 \phi} \quad (7)$$

where, ϕ the volumetric concentration of the flocs ($\phi = c/c_{gel}$), c_{gel} is the gelling concentration at which a space-filling network forms, and c is the sediment concentration by mass. The factor $(1 - \phi_*)$ accounts for the return-flow effect. c/c_{gel} can exceed unity in a consolidating fluid mud layer.

2.2.2. A Model for Turbulence-Induced Flocculation

A complete flocculation model should include both aggregation and floc breakup processes. By assuming a simultaneous acting of aggregation and breakup, the differential equation for the flocculation of cohesive sediment under the influence of turbulent shear, is described with respect to the number concentration, N , as:

$$\frac{\partial N}{\partial t} + \frac{\partial}{\partial x_i} \left(\left(u_i - \delta_{i3} \frac{(1 - \phi)(1 - \phi_p)}{(1 + 2.5\phi)} w_{sr} \right) N \right) - \frac{\partial}{\partial x_i} \left((D_s + \Gamma_T) \frac{\partial N}{\partial x_i} \right) = -k'_A (1 - \phi) G D^3 N^2 + k_B G^{n+1} (D - D_p)^p D^{2n} N \quad (8)$$

where, D_s : molecular diffusivity, Γ_T : turbulent diffusivity, G : the square root of turbulent dissipation rate divided by molecular dynamic viscosity, δ_{i3} : Kronecker's delta. The parameters k'_A and k_B are defined as follows (e.g. Winterwerp, 1998):

$$k'_A = \frac{3}{2} e_c \pi e_d \quad \text{and} \quad k_B = a e_b D_p^{-p} \left(\frac{\mu}{F_y} \right)^q$$

where e_c , e_d , and e_b are efficiency parameters for collision, diffusion, and breakup respectively. μ is the dynamic viscosity of the suspension, F_y is the strength of the mud flocs, and numbers of power, p and q are to be established empirically. The definition and relation of the number concentration, N , and the mass concentration, c , and the volumetric concentration ϕ are:

$$\phi = f_s N D^3 = \frac{c}{\rho_s} \left(\frac{D}{D_p} \right)^{3-n_f} \quad (9)$$

where f_s is the shape factor.

The aggregation and floc breakup terms are set to zero at the water surface and at the horizontal water-bed interface. Hence the boundary conditions lead:

$$\left\{ (u_i - w_s) N - (D_s + \Gamma_T) \frac{\partial N}{\partial x_3} \right\} \Big|_{x_3=Z_s} = 0 \quad \text{and} \quad \left\{ (u_i - w_s) N - (D_s + \Gamma_T) \frac{\partial N}{\partial x_3} \right\} \Big|_{x_3=Z_b} = E_{b,N} \quad (10)$$

The source-sink term $E_{b,N}$ represents the exchange with the bed and is modeled with classical formula of Partheniades and Krone, so that the water-bed exchange formulation is consistent with the one for the mass balance.

3. Application to Jakarta Bay

3.1. Data Collection

Data used for this research are input for hydrodynamic and sediment transport models. The data are: bathymetry, water level, salinity, and temperature, and concentration of total suspended solid.

▪ Bathymetry

Depth data of Jakarta Bay extracted from the World Digital Chart (GEBCO, 2009) as seen in Figure 1.

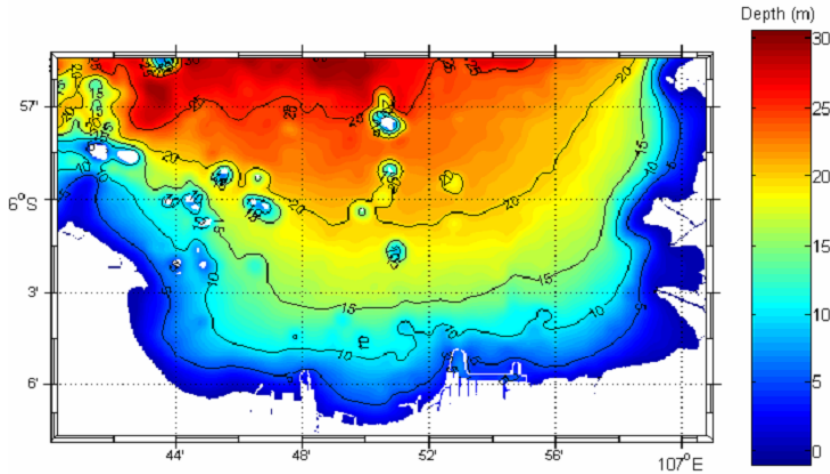


Figure 1. Bathymetry Map of Jakarta Bay.

*Source: GEBCO (2009).

▪ Sea level

Mean sea level data is obtained from prediction of ORI Tide at the northern of Jakarta Bay, at points $106^{\circ} E - 6^{\circ} S$ and $106.967^{\circ} E - 6^{\circ} S$.

▪ Salinity and Temperature

Temperature and salinity data used for initial condition of Jakarta Bay are shown in Table 1.

Table 1. Observed data of average temperature ($^{\circ}C$) and salinity (‰) in the Jakarta Bay.

Parameter	Surface	Bottom
Temperature	33.3	31.2
Salinity	31.6	32.5

*Source: Report of Monitoring Water Quality of Jakarta Bay BPLHD, 2005.

Table 2. Observed data of average temperature ($^{\circ}C$) and salinity (‰) in river mouths.

River mouth	Temperature		Salinity	
	Spring	Neap	Spring	Neap
Angke	32.55	31.3	5	5
Karang	33.1	31.1	18	13
Ancol	32	30,9	20	6

*Source: Report of Monitoring Water Quality of Jakarta Bay BPLHD, 2005.

3.2. Boundary Conditions

Boundary conditions for the model were used at open and river boundaries. The open boundaries are water level, temperature, salinity, and sediment concentration. Water level boundary condition was predicted from tidal

constituents of the Jakarta Bay. River boundary discharges of each river are shown in Table 3, while Table 4 shows for temperature, salinity, and sediment concentration.

Table 4. River discharge.

River mouth	Velocity (m/s)		Discharge (m ³ /s)	
	Spring	Neap	Spring	Neap
M. Angke	-0.060	0.030	-21.6	10.8
M. Karang	0.010	-0.010	3.6	-3.6
M. Ancol	-0.008	0.000	4.6	0.0

Table 5. River boundary conditions.

River mouth	Temperature (°C)		Salinity (‰)		Sediment Concentration (mg/l)
	Spring	Neap	Spring	Neap	
M. Angke	32.5	31.3	5	5	200
M. Karang	33.1	31.1	18	13	200
M. Ancol	32.0	30.9	20	6	200

3.3 Discretisation and Model Desain

Model domain shown in Figure 2, is divided horizontally to 144 x 54 grids and 10 vertical layers. The various parameters used in the numerical simulations are listed in Table 6. as follows :

Simulation of sediment transport was done to identify distribution of sediment around the Jakarta Bay during spring and neap tide. Source of sediment was assumed come from upstream of the three rivers, namely the Muara Angke (A'), Muara Karang (B'), and Muara Ancol (C').

Table 6. Parameter setting.

ΔX	250 m
ΔY	250 m
External interval time	1 s
Internal interval time	10 s
Simulation time	15 days
Initial concentration of TSS	10 mg/l

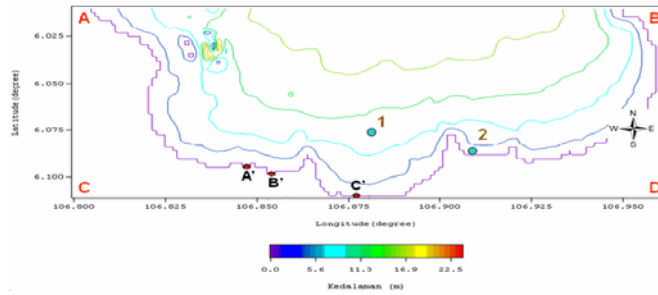


Figure 2. Model domain.

4. Simulation Results of Sediment Transport

Results of sediment transport model are shown in the form of distribution surface concentration during spring tide and neap tide.

4.1. No Wind

4.1.1. Spring Tide

4.1.1.1. Ebb to Flood

Distribution of sediment concentration for ebb to flood condition is shown in Figure 3. The figure shows that high concentration of sediment occurred around river mouths and coastal water near the river mouths. This high concentration was caused by high sediment load from upstream of the rivers. Sediment concentration seaward of the river mouths is small, less than 10 mg/l. From the figure we can see that due to tidal current, sediment from Muara Angke River move eastward.

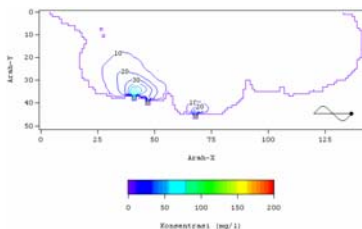


Figure 3. Sediment distribution during ebb to flood condition (spring tide).

4.1.1.2. Flood Tide

Figure 4 shows distribution of sediment concentration during flood condition. Weak current velocity cause deposition of sediment around the river mouths therefore surface sediment concentration is decrease.

4.1.1.3 Flood to Ebb

Strong current during flood to ebb condition increases surface sediment concentration around the river mouths as shown in Figure 5. This strong current is capable to push high concentration of sediment seaward.

4.1.1.4. Ebb Tide

Figure 6 shows distribution of sediment concentration during ebb condition. Distribution of sediment is similar to the previous tidal condition with spreading distance $\pm 6,5$ from the river mouths.

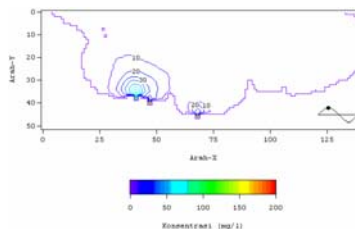


Figure 4. Sediment distribution during flood condition (spring tide).

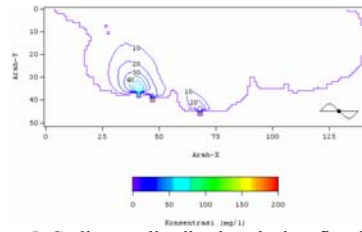


Figure 5. Sediment distribution during flood to ebb condition (spring tide).

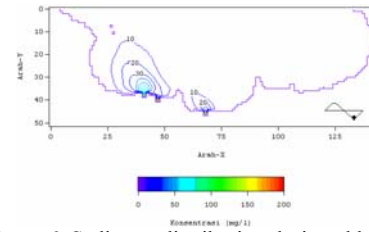


Figure 6. Sediment distribution during ebb condition (spring tide).

4.1.2 Neap Tide

The simulation results during the neap tide condition show similar pattern with the spring tide condition. However, weak current velocity during neap tide causing spreading of sediment is narrower than the

spring tide. Distributions of sediment concentration for neap tide condition are shown in Figures 7-10. Maximum distance of sediment spreading reaches ± 5 km from the river mouths.

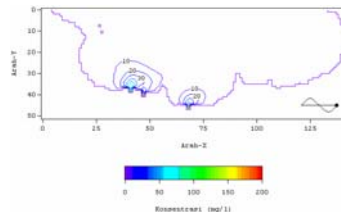


Figure 7. Sediment distribution during ebb to flood condition (neap tide).

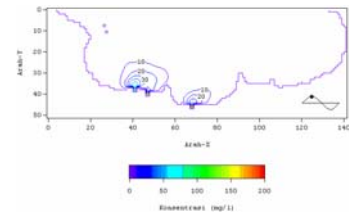


Figure 8. Sediment distribution during flood condition (neap tide).

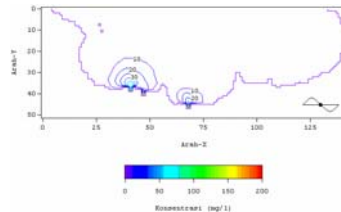


Figure 9. Sediment distribution during flood to ebb condition (neap tide).

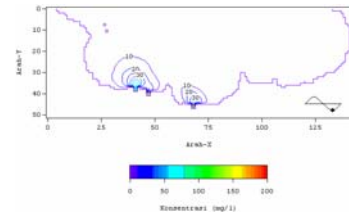


Figure 10. Sediment distribution during ebb condition (neap tide).

4.2. Simulation with Wind

For scenario of simulation with wind data, there are 2 scenarios representing east and west monsoons. Wind speed was assumed to be constant 2 m/s for both scenarios.

4.2.1 West Wind

Simulation results of west wind are shown in Figures 11-14. In this simulation, sediment concentration seems to spread - seaward compared with no wind simulation. Influence of wind seen from direction of sediment spreading to East.

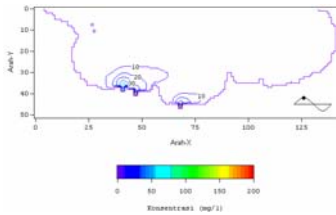


Figure 11. Sediment distribution during flood condition (neap tide).

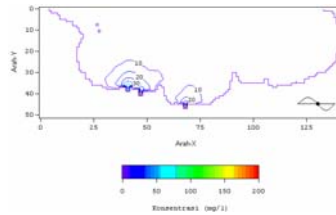


Figure 12. Sediment distribution during flood to ebb condition (neap tide).

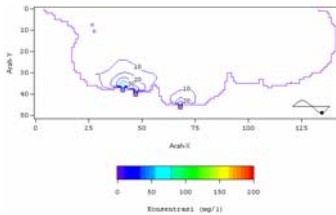


Figure 13. Sediment distribution during ebb condition (neap tide).

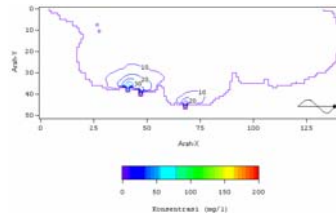


Figure 14. Sediment distribution during ebb to flood condition (neap tide).

4.2.1 East Wind

Simulation results of East Wind are shown in Figures 15-18. In this simulation, sediment concentration g seems to spread seaward compared with no wind

simulation. Influence of wind can be seen from westward spreading of sediment concentration, as shown in Figures 16 and 17.

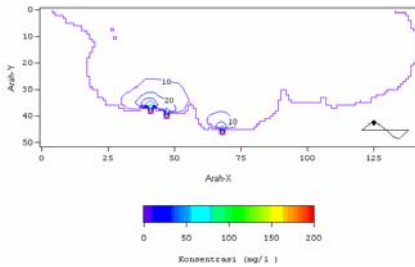


Figure 15. Sediment distribution during flood condition (neap tide).

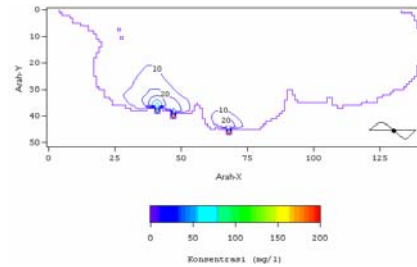


Figure 16. Sediment distribution during flood to ebb condition (neap tide).

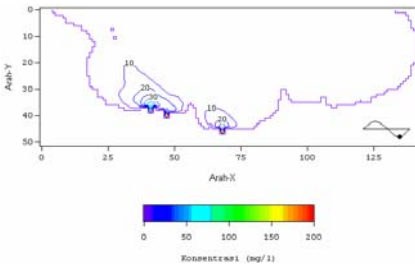


Figure 17. Sediment distribution during ebb condition (neap tide).

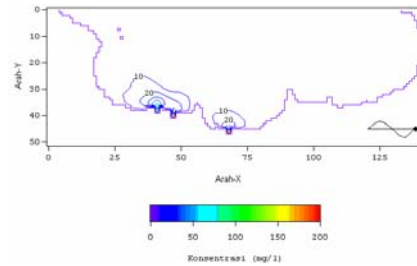


Figure 18. Sediment distribution during ebb to flood condition (neap tide).

4.3 Simulation with Big Discharge

The purpose of this scenario of simulation is to investigate influence of discharge changing to sediment distribution. River discharges used in this simulation were two times of the actual discharges. Simulation results of this scenario are shown in Figures 19-22. From

the figures, we can see that sediments move seaward farther than the actual ones. At the Muara Angke and Muara Karang waters (marked A' and B' in Figure 2, respectively), distance of sediment spreading reaches more than 6 km seaward, while in the Muara Ancol waters (marked C' in Figure 2) it is only ± 2.5 km.

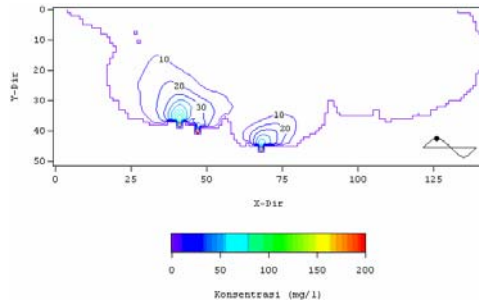


Figure 19. Sediment distribution during flood condition (neap tide).

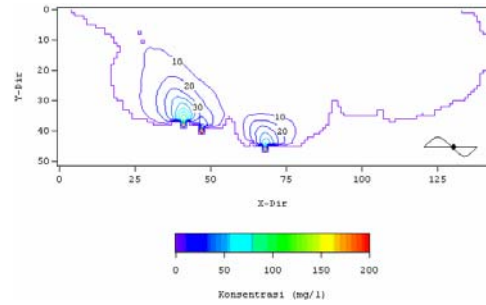


Figure 20. Sediment distribution during flood to ebb condition (neap tide).

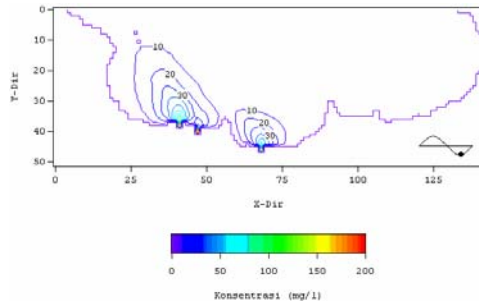


Figure 21. Sediment distribution during ebb condition (neap tide)

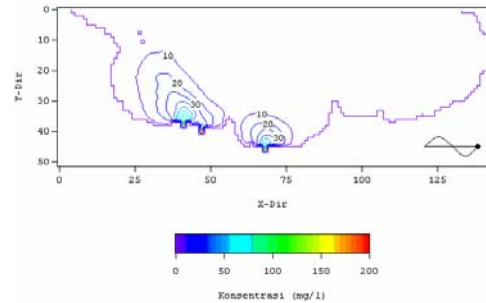


Figure 22. Sediment distribution during ebb to flood condition (neap tide)

5. Distribution of Tidal Current

Generally, all simulation results of current circulation show same pattern. Currents flow from east to west during ebb condition, and flow eastward during flood. Simulation results of current pattern for no wind scenario are shown in Figures 23–26 for spring tide and in Figures 27–30 for neap tide.

Influence of winds to current pattern were small, but they had rather great

influences to sediment distribution. It seems similar influence of discharge to current pattern and sediment distribution. Large Simulation results of wind scenario are shown in Figures 31–34 for West wind and in Figures 35–38 for East wind.

River discharges only gave small influences to current pattern. However, they influence distribution of sediment spreading. The results of simulation are shown in Figures 39–42.

5.1. No Wind (Spring tide)

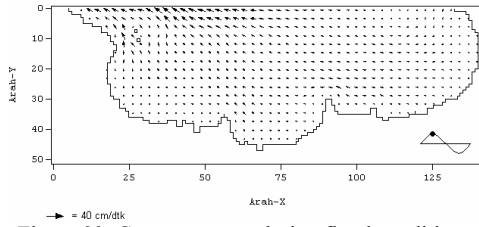


Figure 23. Current pattern during flood condition (spring tide).

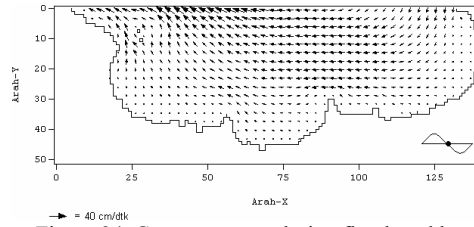


Figure 24. Current pattern during flood to ebb condition (spring tide).

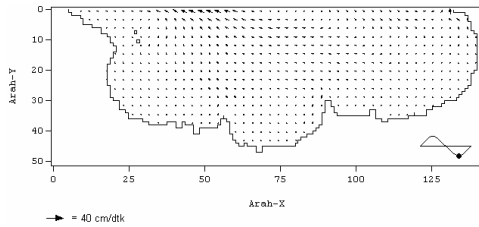


Figure 25. Current pattern during ebb condition (spring tide).

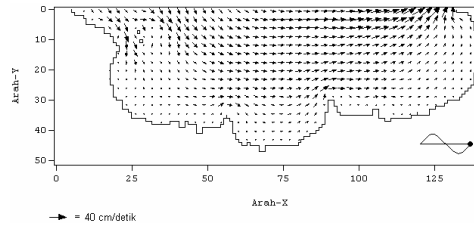


Figure 26. Current pattern during ebb to flood condition (spring tide).

5.2. Wind (Neap Tide)

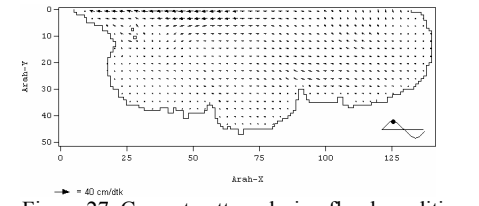


Figure 27. Current pattern during flood condition (neap tide)

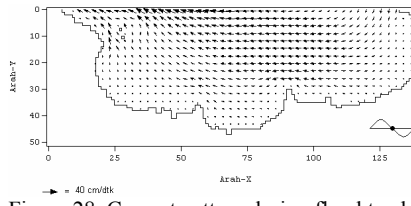


Figure 28. Current pattern during flood to ebb condition (neap tide)

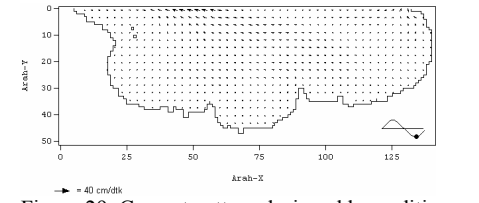


Figure 29. Current pattern during ebb condition (neap tide)

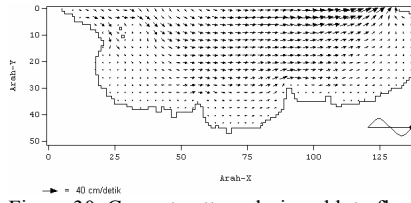


Figure 30. Current pattern during ebb to flood condition (neap tide)

5.3. West Wind

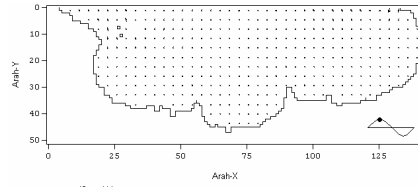


Figure 31. Current pattern during flood condition (neap tide).

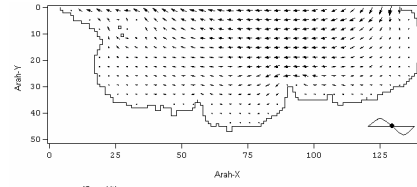


Figure 32. Current pattern during flood to ebb condition (neap tide).

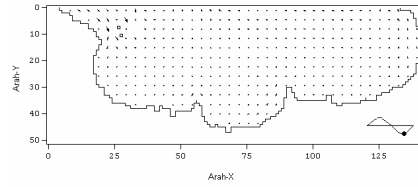


Figure 33 Current pattern during ebb condition (neap tide).

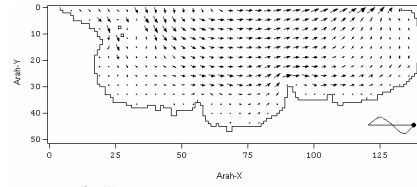


Figure 34. Current pattern during ebb to flood condition (neap tide).

5.4. East Wind

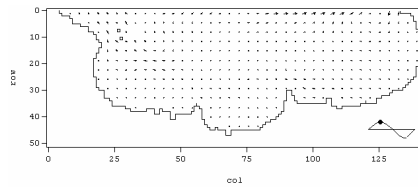


Figure 35. Current pattern during flood condition (neap tide).

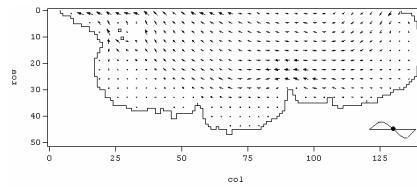


Figure 36. Current pattern during flood to ebb condition (neap tide).

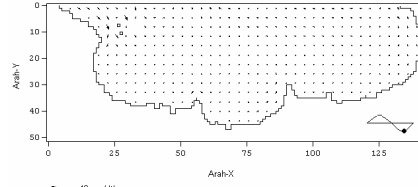


Figure 37. Current pattern during ebb condition (neap tide).

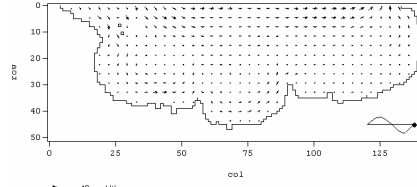


Figure 38. Current pattern during ebb to flood condition (neap tide).

5.5. Large Discharge

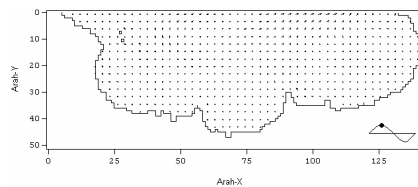


Figure 39. Current pattern during flood condition (neap tide).

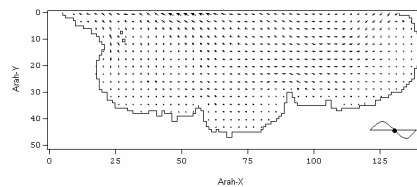


Figure 40. Current pattern during flood to ebb condition (neap tide).

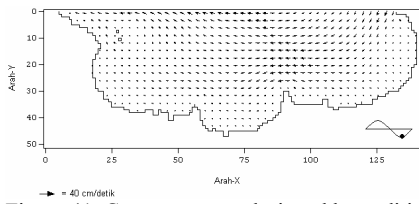


Figure 41. Current pattern during ebb condition (neap tide).

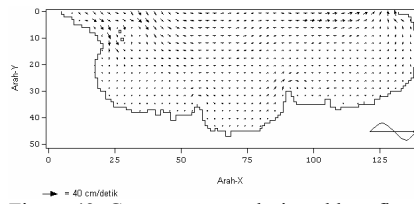


Figure 42. Current pattern during ebb to flood condition (neap tide).

6. Conclusion

In this study, the three-dimensional hydrodynamics and sediment transport model, ECOMSED, have been modified by introducing some method from COSINUS project. The modified model was used for predicting tidal flow and suspended sediment transport in the Jakarta Bay. From the model results we concluded that the models were capable of reproducing the hydrodynamics and cohesive sediment transport processes in the Jakarta Bay. It was found that higher concentration in shallow area occurred due tidal condition and river discharge.

7. References

- Berlamont, J. E. and E. Toorman (eds), 2000, COSINUS Final Scientific Report, Hydraulics Laboratory, K.U. Leuven.
- Bruens, A. W., 2003, Entraining mud suspension, PhD-thesis, Delft University of Technology, Department of Civil Engineering and Geosciences.
- Dyer, K. R., 1997, Estuaries – A Physical Introduction, Wiley.
- HydroQual, 2002, A Primer for ECOMSED Version 1.3, User Manual, HydroQual Inc., New Jersey.
- Koropitan, A. D., Ikeda, M., Damar, A., and Yamanaka, Y., 2009, Influences of physical process on the ecosystem of Jakarta Bay: a coupled physical-ecosystem model experiment, ICES, *Journal of Marine Science*, 66:336-348.
- Rachmayani, R., 2004, 2-D Numerical Model of Horizontal Distribution of BOD-DO by using Quickest Method (manuscript in Bahasa and abstract in English), Final Project, Department of Oceanography, Institut Teknologi Bandung.
- UNESCO, 2000, Reducing megacity impacts on the coastal environment– Alternative livelihoods and waste management in Jakarta and the Seribu Islands, Coastal Region and Small Island Papers 6, UNESCO, Paris, 59 pp.
- Winterwerp, H., 1999, On the dynamics of high-concentrated mud suspension, *Report 99-3 Communication on Hydraulic Engineering*, Department of Civil Engineering and Geosciences, Delft University of Technology.
- Winterwerp, J. C., 2002, On the flocculation and settling velocity of estuarine mud, *Continental Shelf Research*, 22:1339-1360.